



# Solidification and Heat-treatment Conditions Affecting the Tensile Properties and Fracture Feature of an Automotive AlSiMg Alloy

Carolina Barbosa<sup>1</sup> · Hugo Azevedo<sup>1,2</sup> · Sharlane Costa<sup>3</sup> · João Ribeiro<sup>4,5</sup> · José Carlos<sup>2</sup> · Thiago Costa<sup>1</sup> · Otávio Rocha<sup>1,2</sup>

Received: 19 December 2022 / Accepted: 11 March 2023 / Published online: 18 March 2023  
© The Author(s), under exclusive licence to Springer Nature B.V. 2023

## Abstract

In this work, a study on the interrelationship between the solidification and heat-treatment processes parameters with tensile properties and fracture feature was performed with an automotive AlSiMg alloy. For that, samples of the horizontally solidified Al7Si0.3 Mg (wt.%) alloy were subjected to the T6-heat treatment, and tensile tests were performed on both investigated samples, under conditions established from the literature. The solidification conditions such as growth and cooling rates and the secondary dendritic spacing ( $V_L$  and  $T_R$  and  $\lambda_2$ , respectively) and their effects on the ultimate tensile strength ( $\sigma_{UTS}$ ) and elongation (E%) were evaluated. Higher  $\sigma_{UTS}$  values were observed in the heat-treated samples and finer microstructures resulted in a better E% performance. Analysis by SEM/EDS fractography on both samples showed a mix between brittle and ductile fractures, constituted by cleavage facets, secondary cracks, facets covered with micro-voids, tear ridges and dimples. This allowed the deduction of the occurrence of a transition from ductile to brittle fracture along the solidified ingot as well as the predominance of brittle fracture in the heat-treated samples.

**Keywords** Transient solidification · Heat treatment · Microstructure · Fracture · Tensile properties

## 1 Introduction

The use of metallic alloys in the various sectors of engineering and industry is based mainly on mechanical properties, which can be very well programmed. The products by these alloys are able to withstand the loads they are subjected to when in service [1]. It is known that these properties depend largely on the structure which is closely related to chemical compositions and processing conditions, among which heat treatments (HT) are some of the most used [1]. Heat

treatments of metallic alloys are accredited as one of the most important methods of materials manufacturing and developing of new technologies throughout human history. Through controlled heating and cooling operations, the materials properties undergo considerable variations as a result of changes in macrostructure and microstructure characteristics [1].

Grain refinement, dissolution of secondary phases, distribution and morphology changes of phases have been studied over the decades and are linked to the enhancement of mechanical properties in heat treated aluminum alloys [2–6]. Shivkumar, Apelian and collaborators [5, 7, 8] studying Al-Si-Mg alloys observed that HT changes silicon morphology and that the kinetics of spheroidization are affected by the as-cast microstructure. Similarly, addition of sodium, strontium, antimony and bismuth has been investigated as a method of chemical modification of Si-crystal, and studies indicate that machinability, tribology and mechanical properties are significantly affected [9–16].

Recent studies reported that the microstructure scale of directionally solidified as-cast ingots has effects on HT parameters, and plays a crucial role in the extent of morphological transition of the undissolved phases from acicular

✉ Otávio Rocha  
otavio.rocha@ifpa.edu.br

<sup>1</sup> Federal Institute of Education, Science and Technology of Pará-IFPA, Belém, PA 66093-020, Brazil

<sup>2</sup> Faculty of Mechanical Engineering, Federal University of Pará-UFPA, Belém, PA 66075-110, Brazil

<sup>3</sup> University of Minho, 4800-058 Guimarães, Portugal

<sup>4</sup> Polytechnic Institute of Bragança - IPB, 5300-253 Bragança, Portugal

<sup>5</sup> CIMO - Mountain Research Center, 5300-253 Bragança, Portugal

to spheroidized in aluminum alloys [17, 18]. In a previous work published by the authors regarding AlSiMg automotive alloy subjected to T6-heat treatment, it was stated that spheroidized-like eutectic Si particles and Chinese script iron-rich phase were favored after HT in refined microstructure scale conditions, resulting in different behaviors between as-cast and HT samples subjected to responses to microhardness and wear resistance [6, 19].

Microstructural scale, phases morphology and HT are conducive to changes the properties of automotive AlSiMg alloy separately or in conjunction with each other, to develop desired and optimum properties in the casting [20–24]. In this regard, a series of works were recently developed with the automotive casting Al7Si0.3 Mg (wt.%) alloy, which in a first stage aimed to analyze the effects of solidification conditions on the microstructure and mechanical properties [21–23]. In this step, the influence of the thermal solidification parameters, such as growth and cooling rates on the length of the dendritic microstructure as well as on the size, distribution and morphology of the  $Mg_2Si/Fe$  intermetallic compounds (IMCs) and, in turn, on the hardness and tensile properties were investigated. In a second stage [6, 19], T6-heat treatment under different conditions was applied to the as-cast samples resulting from the work of References [21–23].

Studies [20, 21] obtained as-cast ingots of the Al7Si0.3 Mg alloy (wt.%), and typical solidification microstructures observed by both works consisting of a dendritic network with Al-rich primary and secondary phases ( $Al_\alpha$ , Si crystals and IMCs). Finer dendritic microstructures were observed for higher cooling rates values. From the as-cast samples obtained by Lima et al. [21], Souza et al. [22] and Barbosa et al. [23], analyses on the influence of the solidification parameters on the microhardness (HV) of the

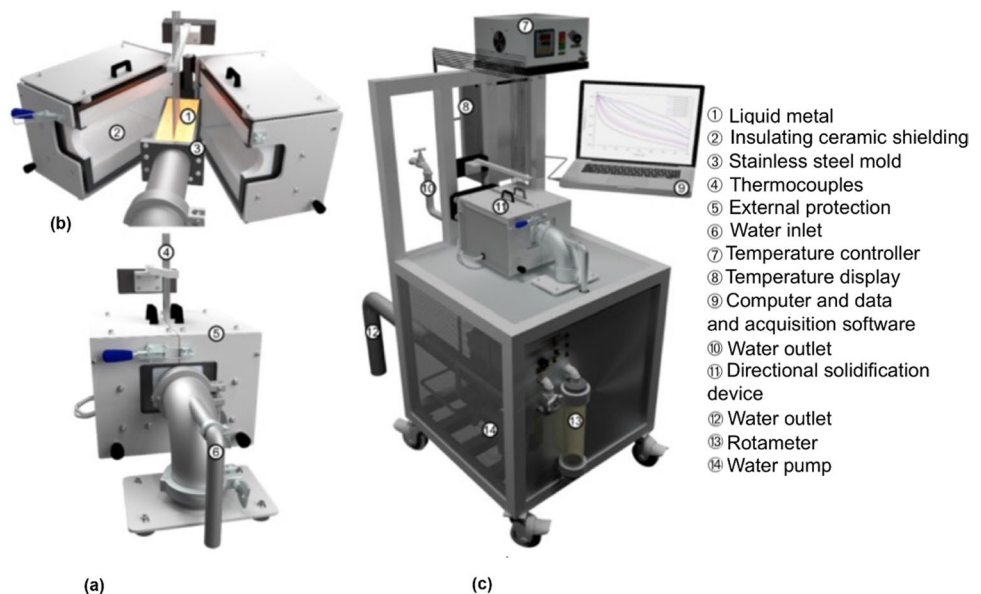
aforementioned alloy were performed. In addition, Souza et al. [22] evaluated the Mg and Cu addition in the Al-7Si alloy (wt.%), depicted higher HV values for the ternary Al-7Si-(0.3 Mg;3Cu) alloys (wt.%), while Barbosa et al. [23] noted higher HV values on IMCs and Si crystals in relation to the Al-rich primary phase ( $Al_\alpha$ ).

More recently, comparative studies on solidification and T6-heat treatment conditions in Al-7Si-xMg (wt.%) cast aluminum alloys have been carried out [6, 18, 19, 24]. Barbosa et al. [6] and Azevedo et al. [19] analyzed the interrelation between the horizontal solidification and treatment processes parameters on the microhardness and wear performance from the work of References [22, 23]. Chen et al. [24] developed investigations to analyze the influence of Mg composition and HT conditions on the mechanical properties of Al-7Si-xMg cast aluminum alloys ( $x \cong 0.26, 0.4$  and  $0.58$  wt.%). In this sense, the present work is a continuity of investigations [6, 18, 21–23] which, although broad, still left a large gap in terms of a more complete mechanical analysis and, thus, aims to present a study on the correlation between tensile properties and microstructural parameters and fracture feature before and after thermal treatment by T6.

## 2 Experimental Procedure

In this work, an Al7Si0.3 Mg alloy ingot (wt.%) was obtained by means of a horizontal water-cooled solidification device. Figure 1 shows a complete assembly scheme of the furnace used in the solidification experiments. The experimental apparatus used to achieve horizontal solidification of studied allo, shown in Fig. 1a, was designed in such a

**Fig. 1** Details of the solidification furnace: **a** and **b** horizontal solidification device showing the water injection system, ingot mold and thermocouples and **c** complete assembly of the horizontal solidification furnace



way that the heat was extracted only through a water-cooled system placed in the lateral mold wall, promoting horizontal solidification. A stainless steel mold was used which was 150 mm of long, 60 mm of wide, 60 mm of high and 3 mm of thick. Experiment was performed with superheat of 10% above the *liquidus* temperature ( $T_L$ ) of Al-7Si-0.3 Mg (wt.%) [6, 19, 21].

Experimental temperature curves were obtained and used to determine the solidification thermal parameters, such as growth and cooling rates ( $V_L$  and  $T_R$ , respectively). Additional details on the operational procedures of the experiments can be consulted in our recently published works [6, 19, 21–23].

In our recent works [6, 19], the precipitation treatment by T6 has been carried out on as-cast samples of the horizontally solidified investigated alloy under the same conditions of this work. It is important to emphasize that the operational parameters for application of the T6-thermal treatment followed guidelines of ASTM-B-597-92-Standard Practice for Heat Treatment of Aluminum Alloys, that is: solution treating performed during 3 h at  $520 \pm 2^\circ\text{C}$ , followed by quenching in warm water ( $70 \pm 2^\circ\text{C}$ ), aging for 1, 2, 3, and 4 h at  $155 \pm 2^\circ\text{C}$  and air-cooling, as shown by the thermal cycles in Fig. 2.

Specimens for tensile tests were prepared from the as-cast ingot, as shown in Fig. 3. In order to guarantee the reproducibility of the results, six samples were prepared

for each position, three for analysis of the solidification conditions ( $V_L$ ,  $T_R$  and  $\lambda_2$ ) and the other three to evaluate the HT conditions. Thus, from the six as-cast specimens, three were submitted to the T6-treatment, according to the thermal cycle of Fig. 2, considering the aging time equal to 3 h, since the highest microhardness value (93.23HV on the Al rich phase) was obtained for this condition [6]. The tests were carried out according to ASTM standards: E384/11 and E8M/04. They have been conducted with a strain rate  $0.05 \text{ mm s}^{-1}$  [25] and the investigated properties include ultimate tensile strength ( $\sigma_{UTS}$ ) and elongation (E%).

In turn, as-cast and HT samples were subjected to microstructural characterization. The length of the microstructural scale was analyzed using secondary dendritic spacing ( $\lambda_2$ ). Once the  $\lambda_2$  values were measured, following the technique from the literature [26, 27], they were correlated with solidification parameters and tensile properties of both investigated samples. Image processing MOTIC system and the Image J software were used to measure the secondary dendrite arm spacings, and at least 20 measurements were taken for each selected position along the casting length. A scanning electron microscope (SEM TESCAM, VEGA LMU) coupled to an energy dispersion spectrum (EDS X-MAX 20, Oxford) was used to investigate fracture feature of both as-cast and heat treated specimens.

**Fig. 2** Thermal cycle showing the operational parameters of the three stages of the T6-treatment

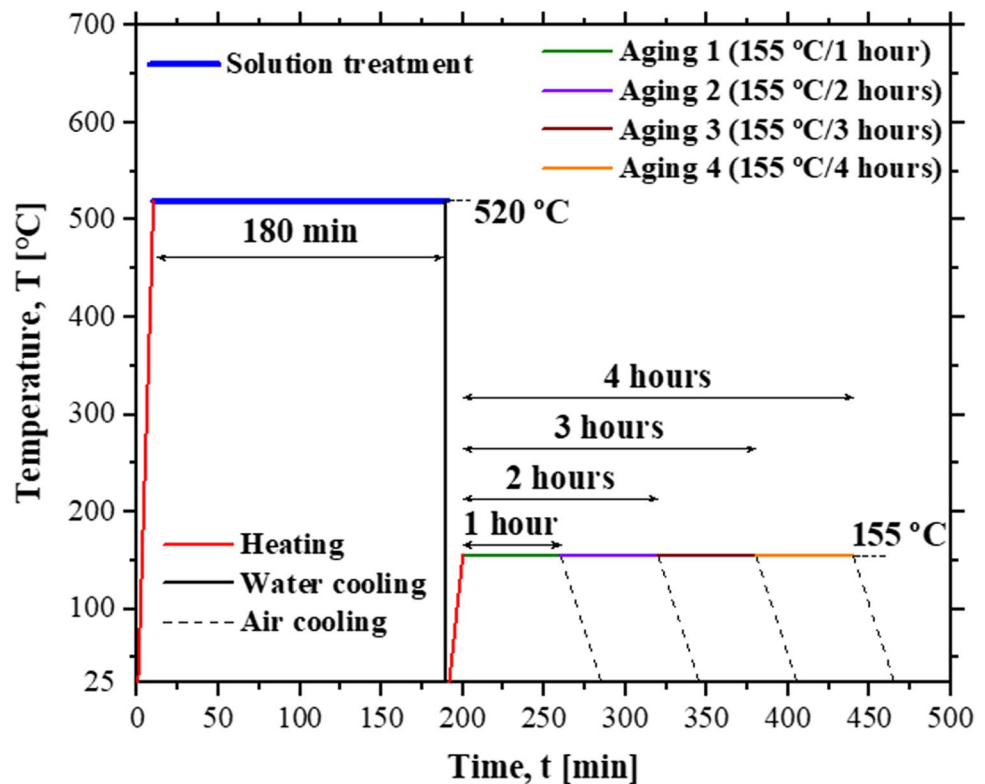
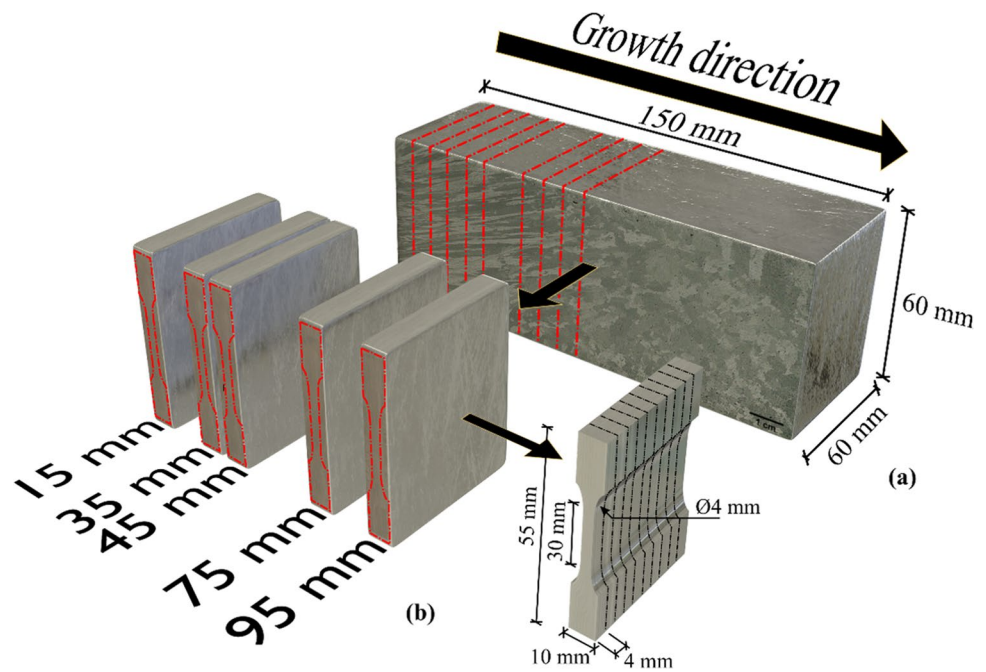


**Fig. 3** **a** As-cast ingot of the investigated alloy, resultant from the solidification process and **b** scheme of sample removal from the ingot resulting for tensile tests



### 3 Results and Discussion

It is known that the solidification thermal parameters exert effects on the length of the microstructural scale. It has been evaluated by the experimental results achieved considering the solidification conditions assumed in the present work, such as the growth and cooling rates ( $V_L$  and  $T_R$ , respectively), which were obtained from experimental thermal data resulting from horizontal. The thermocouples readings, represented by temperature–time profiles shown in Fig. 4a, were used to generate a plot of position from metal/mold interface ( $P$ ) as a function of time ( $t$ ) corresponding to the liquidus front passing by each thermocouple. Very similar experimental points were obtained, and then, a single equation given by  $P = 3(t)^{0.76}$  was proposed. The derivative of this function, that is,  $dP/dt$  provided  $V_L$  values, as shown in Fig. 4b. The experimental  $T_R = f(P)$  profile was calculated by considering the time derivative of each cooling curve right after the passage of the *liquidus* isotherm ( $T_L$ ) by each thermocouple [6, 19, 21–23, 28–30]. It is clearly observed that the cooled mold imposes high  $V_L$  and  $T_R$  values close to the heat transfer interface, which decrease with the increasing formation of the solid layer. Mathematical power equations given by the general expression  $A \cdot P^a$  characterize the  $V_L$  and  $T_R$  variation with the position in the as-cast ingot. This significantly influenced the dendritic network, inheriting finer dendritic microstructures for higher  $V_L$  and  $T_R$  values, as can be seen in Fig. 4c. As observed, it has been represented by experimental power expressions in the forms of  $\text{Constant} \cdot V_L^{-2/3}$  and  $\text{Constant} \cdot T_R^{-1/3}$ , which characterize the  $\lambda_2$  coarsening laws with the solidification thermal parameters.

In our works [6, 19, 21, 23] the  $\lambda_2$  values were measured from the cooled interface, in both as-cast and heat-treated samples, processed under the same conditions assumed in the present work. The expressions resulting from the investigations, which characterize the growth laws of  $\lambda_2$  of the aforementioned samples are presented in Fig. 5. It was observed that the HT has affected the length of the dendritic microstructure scale, since the  $\lambda_2$  values came be greater in the treated samples by T6, as seen in Fig. 5. It was also observed that finer microstructures contributed to the dissolution of the  $\text{Mg}_2\text{Si}$ -intermetallic compound within the Al-rich matrix [6, 19, 24], as well as potentiated the spheroidization process of the eutectic Si crystals during the solution treatment, as depicted by the microstructures above the graph in Fig. 5. Finer microstructures have also allowed better dissolution of  $\text{Al}_2\text{Cu}$  and obtaining spherical-like Si particles during Treatment by T6 in AlSiCu alloys [17, 18, 25, 28].

Figures 6 and 7 present, for both investigated specimens, the results obtained from the tensile tests for two as-cast and heat-treated samples from the heat transfer surface, and studied mechanical properties, respectively. Higher mechanical strengths were achieved for heat-treated samples, as can be seen in Fig. 6a and b. It is observed that the analyzed properties performance along the position in the ingot has not allowed to obtain a mathematical relationship as a function of the solidification parameters ( $V_L$ ,  $T_R$  e  $\lambda_2$ ), especially for the  $\sigma_{UTS}$  values, as seen in Fig. 7a, although finer solidification microstructures have inherited a slight improvement in deformation ( $E\%$ ), as noted in Fig. 7b. This induced the calculation, for

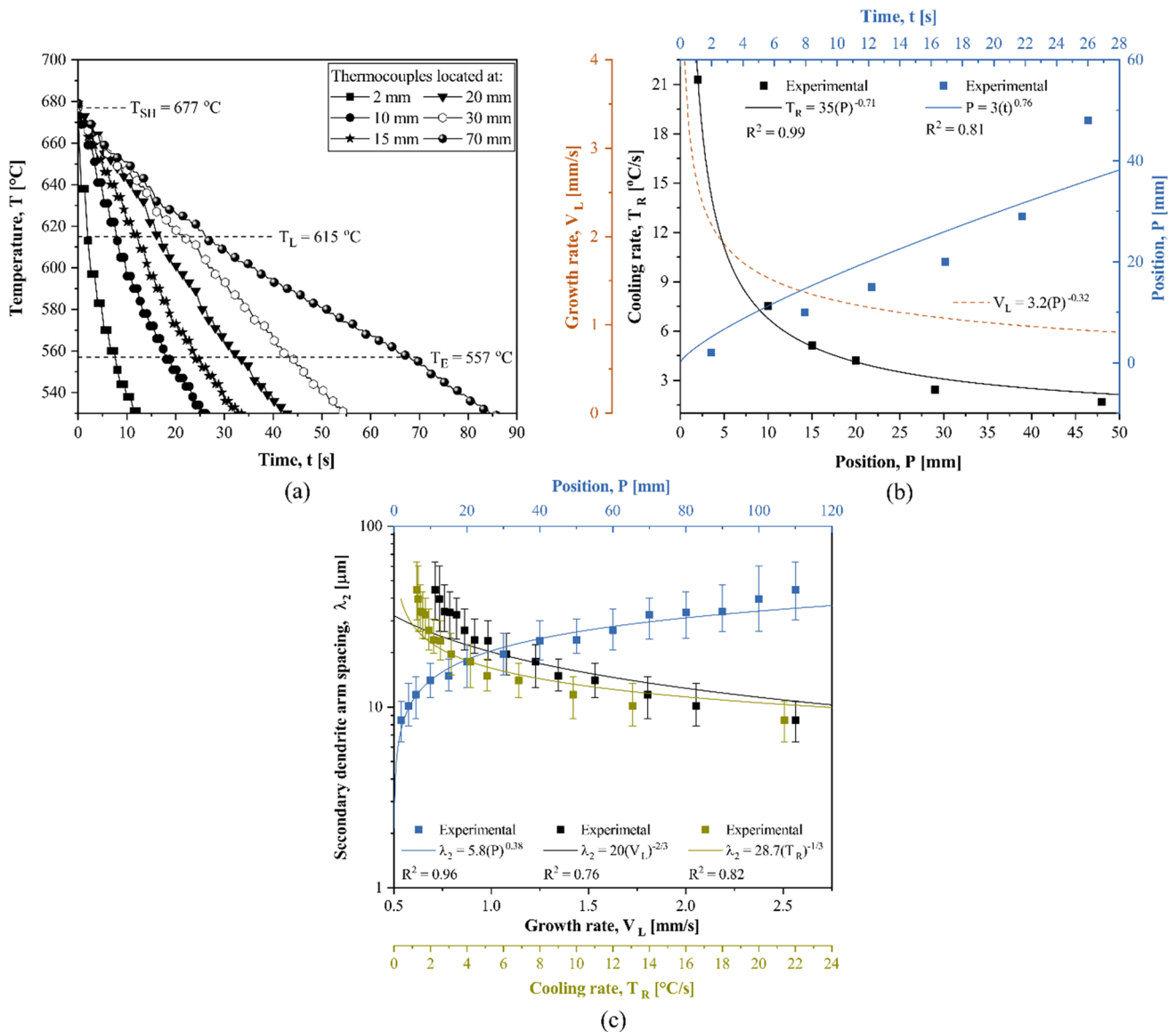


**Fig. 4** Transient thermal and microstructural parameters, resulting from the horizontal solidification process: **a** experimental temperature curves for 6 thermocouples from the heat -transfer interface; **b**

Growth and cooling rates ( $V_L$  and  $T_R$ ); and **c** secondary dendritic spacing ( $\lambda_2$ ) as a function of the position in the ingot,  $V_L$  and  $T_R$ .  $R^2$  is coefficient of determination

both studied samples, of a resulting average value from the averages of each position, as shown in Fig. 7c. High  $\sigma_{UTS}$  and  $E\%$  values can be observed for heat-treated samples, that is, increases from 132.4 to 194.4 MPa ( $\cong 47\%$ ) and 5.8 to 6.1% ( $\cong 5.5\%$ ) have been achieved with the HT, confirming the precipitation hardening without deleterious effects on the deformation. In general, the increase in mechanical resistance achieved with HT does not cause damage to deformation, as can be seen in Fig. 7c. Precipitation hardening also have been observed in the results of HV from the work of Reference [6] for the horizontally solidified and heat-treated Al7Si0.3 Mg alloy in the same conditions of this work.

However, Souza et al. [25] have established an inverse mathematical relationship of  $\sigma_{UTS}$  and  $E\%$  with  $\lambda_2$  for the horizontally solidified Al7Si3Cu alloy, that is, they have observed higher  $\sigma_{UTS}$  and  $E\%$  values for smaller secondary dendrite arm spacing, but HV and yield strength ( $\sigma_{YS}$ ) did not vary with  $\lambda_2$ . In turn, Souza et al. [18] have submitted samples of the horizontally solidified Al7Si3Cu alloy to the T6-heat treatment and observed the hardening of the alloy as well as higher HV values with increasing aging time. An investigation [24] has reported higher  $\sigma_{UTS}$ ,  $\sigma_{YS}$  and  $E\%$  values for finer microstructures in as-cast samples and heat treated by T6 of Al7Si6Mg alloys, also observing higher values of the aforementioned mechanical properties after



**Fig. 5** Comparative curves of  $\lambda_2$  evolution for both analyzed samples, showing microstructural evolution for two positions from the cooled base

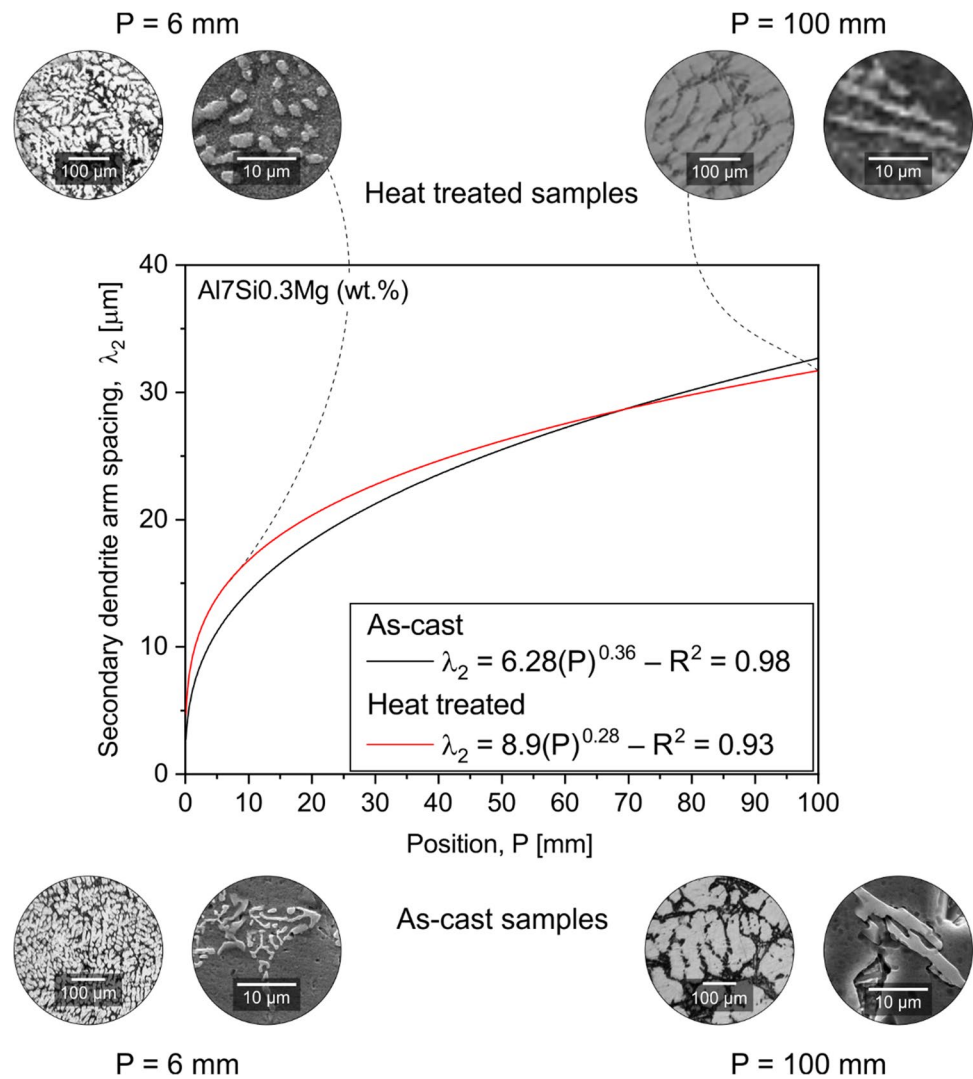
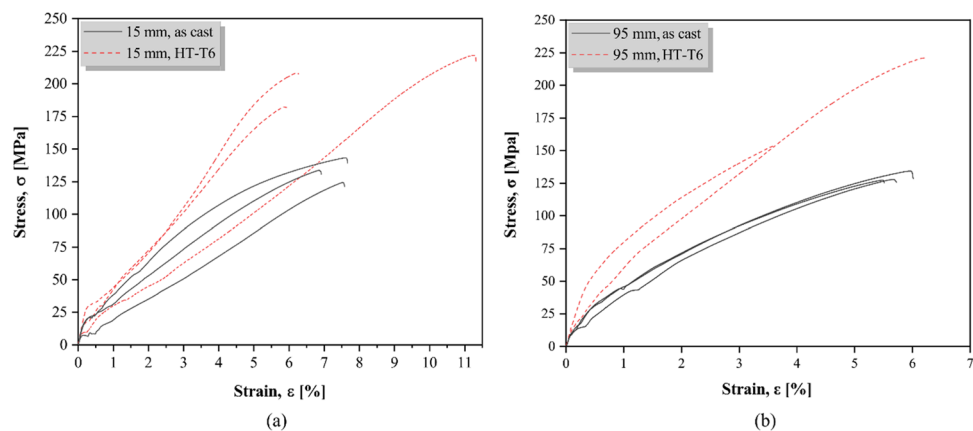


**Fig. 6** Stress x Strain diagrams for two as-cast and heat-treated samples in positions from the cooled base: (15) mm and (b) 75 mm



HT, as well as proposing an inverse mathematical relationship of  $\sigma_{UTS}$ ,  $\sigma_{YS}$  and  $E\%$  with a function of  $\lambda_2$ .

In our research [19], the HT applied under the assumed conditions after solidification process of the investigated

automotive alloy affected the dendritic microstructure scale, since higher  $\lambda_2$  values have been obtained in T6/heat-treated samples. This has influenced the wear resistance of the Al7Si0.3 Mg (wt%) alloy, since lower wear volumes and

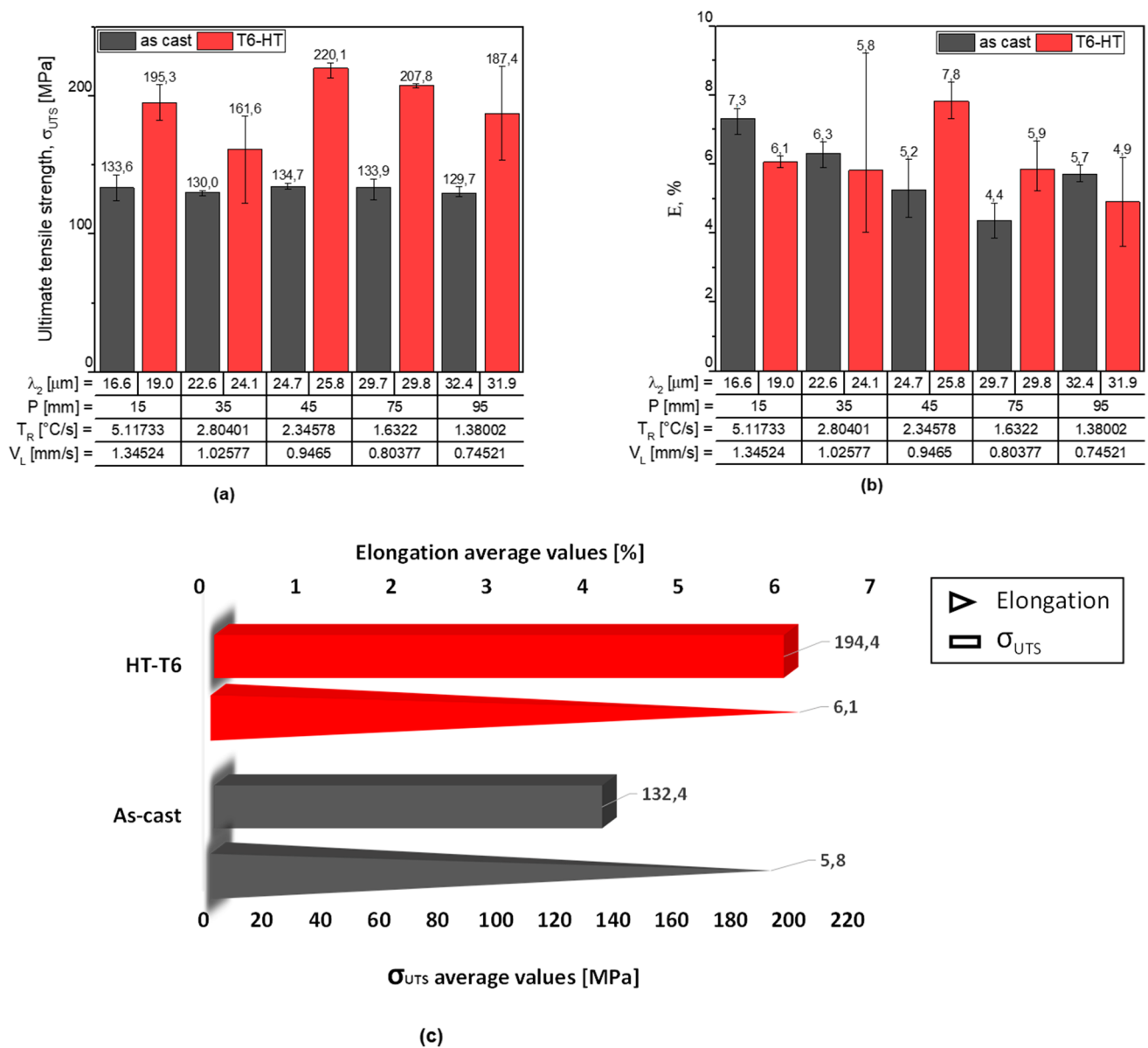


**Fig. 7** Experimental results of the studied properties resulting from the tensile tests: **a** and **b** ultimate tensile strength and elongation vs. solidification parameters, respectively and **c** resulting average values

of ultimate tensile strength and elongation, calculated for all position of both investigated samples

rates were achieved in the as-cast and heat-treated samples for finer and coarser microstructures, respectively. Thus, the results obtained for  $E\%$ , shown in Fig. 7b, in which the finer microstructures present the highest  $E\%$  value, are consistent with the results of the wear behavior for the heat-treated samples [19]. This can also be attributed to the degeneration of tertiary dendritic branches during solution treatment, as observed in [6]. Correlations between wear rate and structure were proposed for as-solidified and heat-treated Al 2 Mg-(5 and 8)Zn (wt%) alloys, and the results, in general, showed that better wear resistance is associated with higher hardness and strength. However, depending on the characteristics of

the microstructure and contact aspects, the wear resistance can have an opposite behavior, inducing the inappropriate selection of the material condition.

A more complex dendritic network of the Al-rich primary phase, consisting of primary, secondary and tertiary branches, may affect the mechanical strength the as-cast alloy. It is known that interdendritic spacing, and the precipitates distributed along the interdendritic regions, acts as strength-increasing mechanisms, creating barriers to dislocation movement during plastic deformation, playing a fundamental role in the tensile results and in the fracture characteristics of metal alloys. In addition, finer dendritic

microstructures can also increase the mechanical strength of as-cast products. The degeneration of the dendritic network with heat treatment, such as the collapse of the tertiary arms, for example, may be decreasing this barrier.

Figures 8, 9, 10, 11 show the SEM images and element scans mapping by EDS of the fractured areas for two as-cast and heat-treated samples, revealed in two samples solidified under different solidification thermal parameters conditions. In general, it is observed that the features of all fracture surfaces of the studied samples indicate a mix between brittle and ductile fractures, constituted by cleavage facets, secondary cracks, facets covered with micro-voids, tear ridges and dimples. In addition, the  $\text{Mg}_2\text{Si}$ /IMCs-like Mg element, initially segregated within the interdendritic regions of the as-cast samples, as noted by scan mappings in Figs. 8 and 10, has been dissolved in the Al-rich matrix during the solution treatment, as can be verified in Figs. 9 and 11 as well as has been reported in our works [6, 19]. Regarding the morphology and fracture modes analysis from the SEM fractographies of as-cast regions, it has shown a predominance and better distribution of small dimples against cleavage facet regions in position close to the heat-transfer surface, deducing the occurrence of a transition from ductile to fragile fracture with decreasing cooling rate as well as with increasing secondary dendritic spacing, as seen in Figs. 8 and 10, respectively. This fracture feature can be associated by the elongation performance observed along the as-cast ingots,

since higher and lower E% values have been obtained for positions near and far from the cooled base, respectively, as reported in Fig. 7b. Souza et al. [25] also reported for the horizontally solidified Al7Si3Cu alloy (wt.%) a transition from ductile to brittle fracture along the position of the as-cast ingot, with the authors attributing it to the decrease in  $T_R$  as well as the increase in  $\lambda_2$ . The increase in the cooling rate and, consequently, the refinement of the dendritic microstructure, have caused transitions in both fracture path from transgranular to intergranular as well as in the fracture mode from quasi-cleavage for dimple [24].

In turn, the presence of dominant cleavage regions is observed in the heat-treated fractured samples, as seen in Figs. 9 and 11, allowing to admit the predominance of brittle fracture in both analyzed positions. It has been observed more extensive cleavage areas in the furthest position from the cooled base, as noted in Fig. 11. This has inherited a deformation behavior similar to that observed in as-cast samples, i.e., lower E% values have been achieved in heat-treated positions far from the heat-transfer surface, as can be seen in Fig. 7b.

Therefore, the cleavage planes seem to be closely associated with the silicon crystals present in the microstructure, thus, the larger and more faceted the Si particles, the fracture will tend to be more brittle, with a predominance of cleavage planes, whereas when refining and spheroidizing the Si-crystals, ductile fracture mechanism will prevail. Was observed

**Fig. 8** SEM fractographies and elemental scanning mapping by EDS for both investigated as-cast samples in the ingot equal to 15 mm

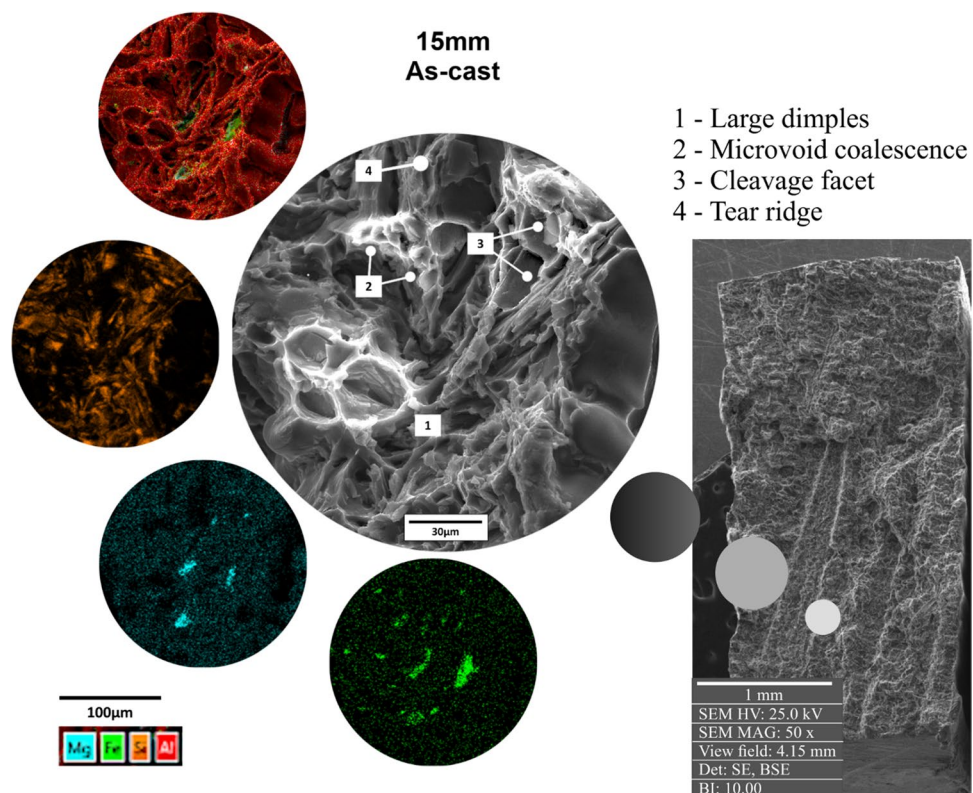




**Fig. 9** SEM fractographies and elemental scanning mapping by EDS for both investigated HT samples in the ingot equal to 15 mm

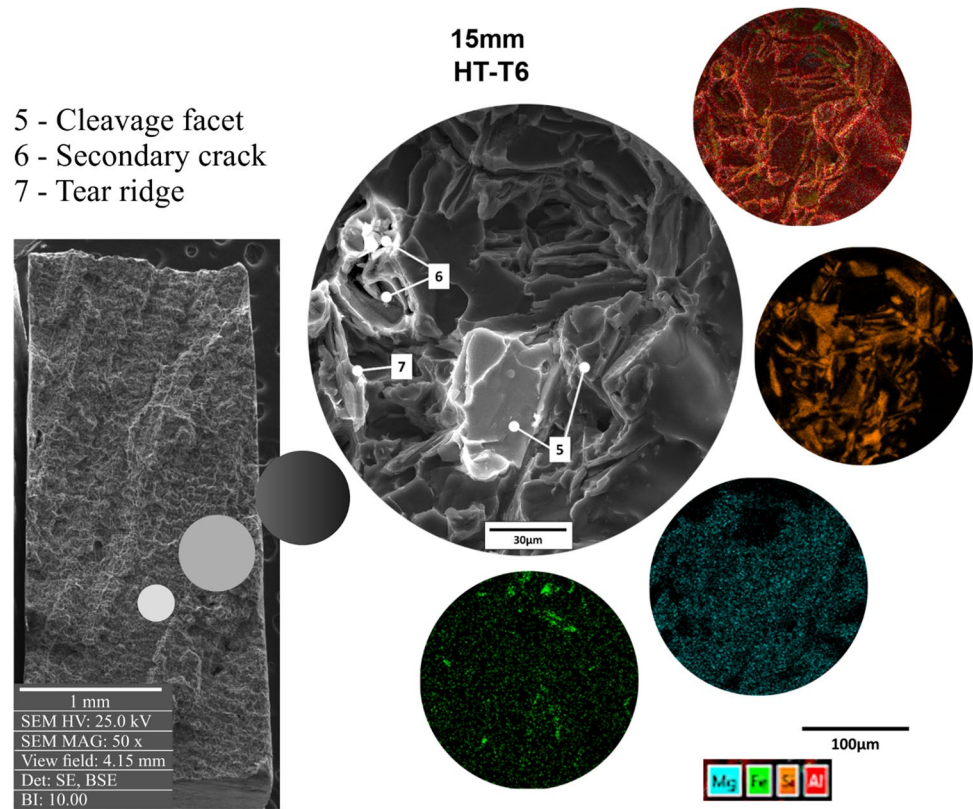
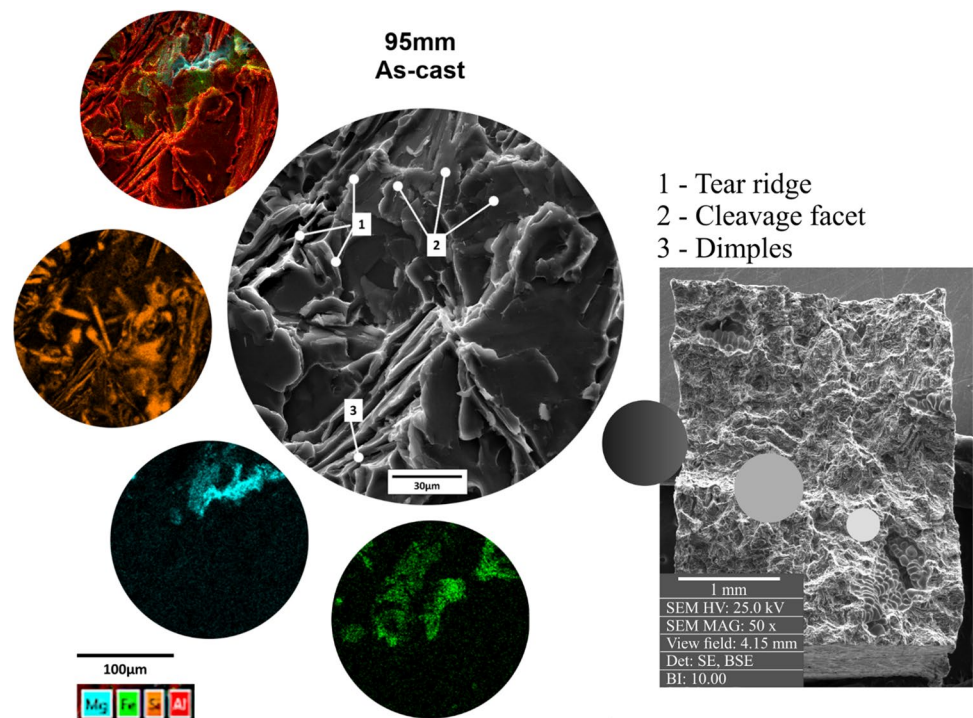


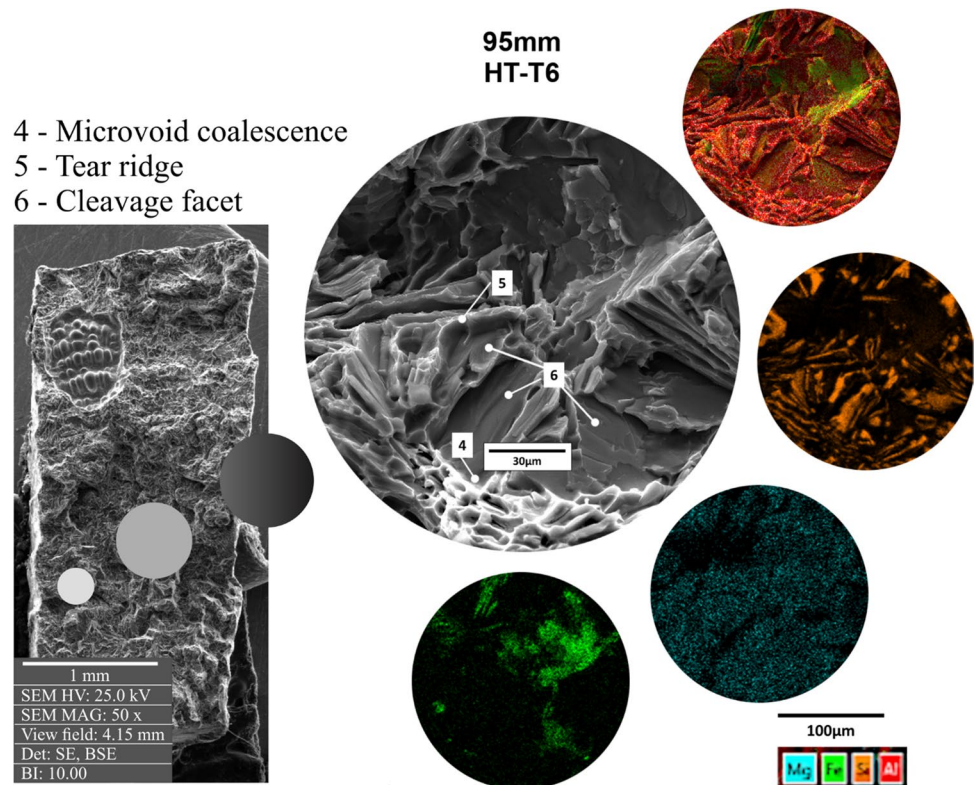
**Fig. 10** SEM fractographies and elemental scanning mapping by EDS for both investigated as-cast samples in the ingot equal to 95 mm



that the presence of  $\text{Mg}_2\text{Si}$ -IMC increases the density of dimples in fracture surfaces possibly because this phase acts as a deformation energy absorber, promoting controlled

nucleation of microvoid in the interdendritic region. On the other hand, for HT specimens the  $\text{Mg}_2\text{Si}$ -IMC particles are solubilized from the interdendritic region to the  $\alpha$ -Al matrix,

**Fig. 11** SEM fractographies and elemental scanning mapping by EDS for both investigated HT samples in the ingot equal to 95 mm



leading a direct interaction between Si-crystal (high elasticity module) and  $\alpha$ -Al phase (low elasticity module), increasing the occurrence of brittle fracture.

## 4 Conclusion

The main conclusions obtained from this study are:

1. Ultimate tensile strength values were achieved for heat-treated samples, proving the effectiveness of HT under the assumed conditions. Despite the hardening of the Al-rich matrix, this has not influenced the elongation performance, since in general the E% values remained very close in both investigated samples, even being slightly better.
2. Under the assumed conditions, finer microstructures have inherited better deformation conditions for both solidification and heat-treatment samples.
3. Analysis from the SEM/EDS fractographs of both as-cast and heat-treated samples has shown a perfect dissolution of the  $\text{Mg}_2\text{Si}$ -IMCs in the matrix during the solution heat treatment. In addition, EDS scan mappings have depicted finer Si and Fe particles in a-cast samples, for higher and lower  $T_R$  and  $\lambda_2$  values, respectively. This has inherited better conditions for obtaining spherical-

like Si crystals after the solution treatment and probably contributed to the good E% performance.

4. From the analysis of fracture features performed on both as-cast and heat-treated samples, it was observed by the fracture morphologies in the as-cast samples the predominant presence of dimples and cleavage for finer and coarser microstructures, respectively, deducing the occurrence of a transition from ductile to brittle fracture modes along the length of the ingot. While in samples treated by T6, cleavage areas became prominent, suggesting a predominance of brittle fracture.

**Acknowledgements** The authors acknowledge the support provided by IFPA—Federal Institute of Education, Science and Technology of Pará—Campus Belém, to the Polytechnic Institute of Bragança for the master's degree and international exchange of the student Carolina Rizzioli Barbosa, respectively, and UFPA—Federal University of Pará.

**Author Contributions** All authors contributed to the study conception and design. Material preparation, data collection and analysis were performed Carolina Rizzioli Barbosa, Hugo André Magalhães de Azevedo, Sharlane Costa, João Eduardo Pinto Castro Ribeiro, José Carlos de Araújo Cardoso Filho, Thiago Antônio Paixão de Sousa Costa, and Otávio Fernandes Lima da Rocha. The first draft of the manuscript was written by Otávio Fernandes Lima da Rocha and all authors commented on previous versions of the manuscript. All authors read and approved the final manuscript.

**Funding** The authors listed below are grateful for the financial support provided by the following foundations:

(1) Otávio Fernandes Lima da Rocha: CNPq—National Council for Scientific and Technological Development (Grants 302846/2017-4).

(2) Sharlane Costa and João Ribeiro: Foundation for Science and Technology (FCT, Portugal) for financial support by national funds FCT/MCTES to CIMO (UIDB/00690/2020).

**Data Availability** All data generated or analysed during this study are included in this published article.

## Declarations

**Consent for Publication** Not applicable.

**Competing Interests** The authors declare no competing interests

## References

- Chiaverini V (2003) Tratamento térmico das ligas metálicas. Associação Brasileira de Metalurgia e Materiais, São Paulo
- Onurlu S, Tekin A (1994) Effect of heat treatment on the insoluble intermetallic phases present in an AA 6063 alloy. *J Mater Sci*. <https://doi.org/10.1007/BF00368940>
- Sjölander E, Seifeddine S (2010) The heat treatment of Al–Si–Cu–Mg casting alloys. *J Mater Process Technol*. <https://doi.org/10.1016/j.jmatprot.2010.03.020>
- Marioara CD, Andersen SJ, Jansen J, Zandbergen HW (2003) The influence of temperature and storage time at RT on nucleation of the  $\beta$  phase in a 6082 Al–Mg–Si alloy. *Acta Mater*. [https://doi.org/10.1016/S1359-6454\(02\)00470-6](https://doi.org/10.1016/S1359-6454(02)00470-6)
- Apelian D, Shivkumar S, Sigworth G (1989) Fundamental aspects of heat treatment of cast Al–Si–Mg alloys. *AFS Trans* 97:727–742
- Barbosa CR, Machado GH, Azevedo HM, Rocha FS, José Filho C, Pereira AA, Rocha OL (2020) Tailoring of processing parameters, dendritic microstructure, Si/intermetallic particles and microhardness in as-cast and heat-treated samples of Al7Si0.3Mg alloy. *Met Mater Int*. <https://doi.org/10.1007/s12540-019-00334-y>
- Shivkumar S, Ricci S Jr, Apelian D (1990) Influence of solution parameters and simplified supersaturation treatments on tensile properties of A356 Alloy. *AFS Trans* 98:913–922
- Shivkumar S, Ricci S Jr, Steenhoff B, Apelian D, Sigworth G (1989) An experimental study to optimize the heat treatment of A356 alloy. *AFS Trans* 97:791–810
- Bian XF, Wang WM, Qin JY (2000) Structures of liquid Al–Si alloy modified by Sr. *Mater Sci Forum*. <https://doi.org/10.4028/www.scientific.net/MSF.331-337.349>
- Liao H, Sun Y, Sun G (2002) Correlation between mechanical properties and amount of dendritic  $\alpha$ -Al phase in as-cast near-eutectic Al–11.6% Si alloys modified with strontium. *Mater Sci Eng A*. [https://doi.org/10.1016/S0921-5093\(01\)01949-9](https://doi.org/10.1016/S0921-5093(01)01949-9)
- Shivkumar S, Ricci S, Keller C, Apelian D (1990) Effect of solution treatment parameters on tensile properties of cast aluminum alloys. *J Heat Treat*. <https://doi.org/10.1007/BF02833067>
- Farahany S, Ourdjini A, Idris MH, Thai LT (2011) Effect of bismuth on microstructure of unmodified and Sr-modified Al–7Si–0.4 Mg alloys. *Trans Nonferrous Met Soc China*. [https://doi.org/10.1016/S1003-6326\(11\)60881-9](https://doi.org/10.1016/S1003-6326(11)60881-9)
- Dias M, Oliveira R, Kakitani R, Cheung N, Henein H, Spinelli JE, Garcia A (2020) Effects of solidification thermal parameters and Bi doping on silicon size, morphology and mechanical properties of Al–15wt.%Si–3.2wt.%Bi and Al–18wt.%Si–3.2wt.%Bi alloys. *J Mater Res Technol*. <https://doi.org/10.1016/j.jmrt.2020.01.083>
- Costa TA, Dias M, Silva C, Freitas E, Silva AP, Cheung N, Garcia A (2019) Measurement and interrelation of length scale of dendritic microstructures, tensile properties, and machinability of Al–9wt.%Si–(1wt.%Bi) alloys. *Int J Adv Manuf Technol*. <https://doi.org/10.1007/s00170-019-04211-1>
- Farahany S, Ourdjini A, Bakar TA, Idris MH (2014) Role of bismuth on solidification, microstructure and mechanical properties of a near eutectic Al–Si alloys. *Met Mater Int*. <https://doi.org/10.1007/s12540-014-5019-5>
- Wu X, Zhang G, Wu F (2013) Influence of Bi addition on microstructure and dry sliding wear behaviors of cast Al–Mg2Si metal matrix composite. *Trans Nonferrous Met Soc China*. [https://doi.org/10.1016/S1003-6326\(13\)62627-8](https://doi.org/10.1016/S1003-6326(13)62627-8)
- Costa TA, Dias M, Gomes LG, Rocha OL, Garcia A (2016) Effect of solution time in T6 heat treatment on microstructure and hardness of a directionally solidified Al–Si–Cu alloy. *J Alloys Compd*. <https://doi.org/10.1016/j.jallcom.2016.05.099>
- Souza FA, Costa MO, Magno IA, Nascimento JM, Silva AP, Costa TS, Rocha OL (2019) Investigation on microstructural and microhardness evolution in as-cast and T6/heat-treated samples of a horizontally solidified AlSiCu alloy. *J Mater Res Technol*. <https://doi.org/10.1016/j.jmrt.2019.06.054>
- Azevedo HM, Botelho TM, Barbosa CR, Sousa AP, Costa TA, Rocha OL (2020) Study of drywear behavior and resistance in samples of a horizontally solidified and T6/heat-treated automotive AlSiMg alloy. *Tribol*. <https://doi.org/10.1007/s11249-020-01302-z>
- Chen R, Shi Y, Xu Q, Liu B (2014) Effect of cooling rate on solidification parameters and microstructure of Al–7Si–0.3 Mg–0.15 Fe alloy. *Trans Nonferrous Met Soc China*. [https://doi.org/10.1016/S1003-6326\(14\)63236-2](https://doi.org/10.1016/S1003-6326(14)63236-2)
- Lima JO, Barbosa CR, Magno IAB, Nascimento JM, Barros AS, Oliveira MC, Souza FA, Rocha OL (2018) Microstructural evolution during unsteady-state horizontal solidification of Al–Si–Mg (356) alloy. *Trans Nonferrous Met Soc China*. [https://doi.org/10.1016/S1003-6326\(18\)64751-X](https://doi.org/10.1016/S1003-6326(18)64751-X)
- Souza F, Lima J, Rizzioli C, Magno I, Barros A, Moreira A, Rocha O (2018) Microstructure and microhardness in horizontally solidified Al–7Si–0.15 Fe–(3Cu; 0.3 Mg) alloys. *Mater Sci Technol*. <https://doi.org/10.1080/02670836.2018.1444923>
- Barbosa CR, Lima JOM, Machado GMH, Azevedo HAM, Rocha FS, Barros AS, Rocha OFL (2019) Relationship between aluminum-rich/intermetallic phases and microhardness of a horizontally solidified AlSiMgFe alloy. *Mater Res*. <https://doi.org/10.1590/1980-5373-MR-2018-0365>
- Chen R, Xu Q, Guo H, Xia Z, Wu Q, Liu B (2017) Correlation of solidification microstructure refining scale, Mg composition and heat treatment conditions with mechanical properties in Al–7Si–Mg cast aluminum alloys. *Mater Sci Eng A*. <https://doi.org/10.1016/j.msea.2016.12.051>
- Souza FA, Magno IA, Costa MO, Barros AS, Nascimento JM, Carvalho DB, Rocha OL (2019) Unsteady-state horizontal solidification of an Al–Si–Cu–Fe alloy: relationship between thermal parameters and microstructure with mechanical properties/fracture feature. *Met Mat Int*. <https://doi.org/10.1007/s12540-018-0174-8>
- Çadırlı E (2013) Effect of solidification parameters on mechanical properties of directionally solidified Al-rich Al–Cu alloys. *Met Mater Int*. <https://doi.org/10.1007/s12540-013-3006-x>
- McCartney DG, Hunt JD. Measurements of cell and primary dendrite arm spacing in directionally solidified aluminium alloys. *Acta Metall*. [https://doi.org/10.1016/0001-6160\(81\)90111-5](https://doi.org/10.1016/0001-6160(81)90111-5)
- Magno IA, Souza FA, Costa MO, Nascimento JM, Silva AP, Costa TS, Rocha OL (2019) Interconnection between the solidification and precipitation hardening processes of an AlSiCu alloy. *Mat Sci Technol*. <https://doi.org/10.1080/02670836.2019.1591028>
- Nascimento MS, Franco ATR, Frajuca C, Nakamoto FY, Santos GAD, Couto AA (2018) An experimental study of the



- solidification thermal parameters influence upon microstructure and mechanical properties of Al-Si-Cu alloys. *Mater Res.* <https://doi.org/10.1590/1980-5373-MR-2017-0864>
30. Ache C, Lopes M, Reis B, Garcia A, Santos CD (2020) Dendritic spacing/columnar grain diameter of Al–2Mg–Zn alloys affecting hardness, tensile properties, and dry sliding wear in the as-cast/heat-treated conditions. *Adv Eng Mater.* <https://doi.org/10.1002/adem.201901145>
- Publisher's Note** Springer Nature remains neutral with regard to jurisdictional claims in published maps and institutional affiliations.
- Springer Nature or its licensor (e.g. a society or other partner) holds exclusive rights to this article under a publishing agreement with the author(s) or other rightsholder(s); author self-archiving of the accepted manuscript version of this article is solely governed by the terms of such publishing agreement and applicable law.